


RESEARCH

Open Access



Shear Behavior of Reactive Powder Concrete Ferrocement Beams with Light Weight Core Material

Mohamed H. Makhlouf^{1*} , M. Alaa¹, Gamal I. Khaleel¹, K. M. Elsayed¹ and M. H. Mansour¹

Abstract

In this paper, the shear behavior of ferro-cement hollow beams is investigated experimentally and analytically. Ten reinforced concrete beams with cross-sectional dimensions of 100 × 200 × 1300 mm and a clear span of 1000 mm were cast and tested until failure under a two-point loading system. Ferrocement beams in this research contained either an autoclaved aerated lightweight brick core (AAC) or an extruded foam core (EFC) and were reinforced with either expanded metal mesh (EMM) or welded wire mesh (WWM). The structural behavior of the studied beams, including first crack, deflection, ultimate load, crack pattern, failure mode, and ductility index, was investigated. The experimental data were used to validate finite element models created with the ABAQUS finite element program. It can be concluded that the optimum performance of ferrocement beams can be achieved using beams with a second layer of expanded steel mesh as additional reinforcement, which led to an increase in the ultimate load and maximum deflection by 12.9% and 22.8%, respectively. Furthermore, the Numerical results agreed with the experimental results, where the ratio between the NLFE ultimate loads and the experimental ultimate loads varies between 1.02 and 1.07, with an average ratio of 1.04.

Keywords Ferrocement, Shear strength, Expanded wire mesh, Welded wire mesh, ABAQUS finite element program

1 Introduction

Ferrocement (FC) is defined as wire mesh reinforcement impregnated with mortar to produce elements of small thickness, high durability and resilience, and, when properly shaped, high strength and rigidity. Many researchers have been conducted on the ferrocement as a low-cost construction material and a flexible structural system, and many parameters were carried out to validate the new system and to enhance its performance. There is a sizable demand for strengthening concrete structures worldwide, and there are several reasons for

this. Deterioration brought on by aging and environmental exposure, rising society's more significant traffic, or functional changes like a higher required permit load frequently causes deficiencies (Al-Numan et al., 2016; Al-Shathr et al., 2022).

Ferrocement presents the opportunity to construct relatively light prefabricated structural elements that can be shaped into intriguing building shapes for affordable housing. For concrete reinforcement, buildings, tanks, roofs, silos, and other structures have all been built or repaired using ferrocement (Gaidhankar et al., 2017; Shaheen et al., 2022; Suresh, 2004; Usman & Shahrudin, 2018). The main applications of ferrocement are the reinforcement of columns, beams, and slabs made of reinforced concrete (Kaish et al., 2018; Shaaban et al., 2018a; Yardim, 2019). However, due to its thinness and labor-intensive manufacturing process, its acceptability in Malaysia is being held up (Abang,

Journal information: ISSN 1976-0485 / eISSN 2234-1315.

*Correspondence:

Mohamed H. Makhlouf
mohamedmakhlouf83@yahoo.com

¹ Civil Department, Benha Faculty of Engineering, Benha University, Benha, Egypt



© The Author(s) 2024. **Open Access** This article is licensed under a Creative Commons Attribution 4.0 International License, which permits use, sharing, adaptation, distribution and reproduction in any medium or format, as long as you give appropriate credit to the original author(s) and the source, provide a link to the Creative Commons licence, and indicate if changes were made. The images or other third party material in this article are included in the article's Creative Commons licence, unless indicated otherwise in a credit line to the material. If material is not included in the article's Creative Commons licence and your intended use is not permitted by statutory regulation or exceeds the permitted use, you will need to obtain permission directly from the copyright holder. To view a copy of this licence, visit <http://creativecommons.org/licenses/by/4.0/>.

1995). Larger international organizations, including the RILEM (International Union of Construction and Laboratories Materials, Structure Experts, and Systems) and the FIB (Structural Concrete Federation), have not yet adopted or sponsored ferrocement, which is limited to ferrocement (Naaman, 2015).

Abdullah and Abdulla (2022) looked into the first crack load, ultimate load, and energy absorption increase by (20%, 30.25%, and 69.2%) for ferrocement beams reinforced with steel bars and steel wire mesh and by (34.36%, 27.1%, 94.92%) for ferrocement beams reinforced with GFRB bars and fiber glass mesh when three layers of mesh are used, respectively, when compared to beams reinforced with bars alone without mesh. Also, for most of the examined steel-reinforced beams, there is a fair agreement between the theoretical ultimate loads and the experimental data.

Alobaidy et al. (2022) looked into all ferrocement beams reinforced with glass mesh, which had an ultimate deflection that was somewhat lower than that of ferrocement reinforced with steel mesh. Furthermore, all ferrocement reinforced with welded mesh had lower initial fracture loads than ferrocement beams reinforced with fiberglass mesh. Comparing ferrocement reinforced with fiberglass meshes (1, 2, and 3 layers) to ferrocement reinforced with welded steel meshes (1, 2, and 3 layers) revealed reductions in the ultimate load of 3.27%, 16.52%, and 9.38%, respectively. However, the ultimate load of this ferrocement was enhanced by 33.71%, 73.28%, and 122.11%, respectively, compared to ferrocement that was not strengthened against shear. Furthermore, compared to ferrocement that was not reinforced to withstand shear with mortar alone, the maximum load of ferrocement reinforced utilizing layers of welded mesh was enhanced by 38.23%, 107.56%, and 145.09%, respectively. Additionally, the number and width of fractures decreased when steel stirrups were replaced with fiberglass and steel mesh, especially in ferrocement beams reinforced with two and three layers of mesh.

Nasr (2019) investigated using a ferro-cement layer with expanded galvanized metal steel mesh, a 15×40 mm opening, and a 2.5 mm wire thickness. According to the experimental findings, adding ferro-cement to a structure strengthened its load capacity by 23%. An experimental approach was used to investigate the effects of different types of reinforcement on the flexural behavior of thin hollow-core slabs made of ferrocement with PVC pipes inserted (Naser et al., 2021). Of all the slabs tested, the one reinforced just with macro-steel fibers had the highest flexural strength and the lowest deflection. In contrast, the slab reinforced with steel bars had the maximum stiffness.

El-Sayed and Erfan (2018) enhanced the shear behavior of composite ferrocement beams. Results indicated that expanded wire mesh beams had a higher shear capacity than beams made of reference and welded wire mesh. It has been demonstrated that using ferrocement as permanent formwork, especially for curved structures, has tremendous potential for accelerating construction and maximizing materials at a low cost. It also has the advantage of decreasing the amount of reinforcement for tension required in slabs and beams by employing steel meshes that raise the ability of the structural elements to withstand tension (Fahmy et al., 2014).

In testing on ferrocement beams, Rao et al. (2006) changed the effective depth-to-shear span ratio (a/d) and tested for various mesh layers. The shear capacity of the member was shown to rise with an increase in the volume percentage of the mesh reinforcement. Additionally, it has been discovered that shear behavior predominates up to a shear span to an effective depth ratio of 3. When the flexural behavior is dominant, and the shear span-to-depth ratio is greater than 3, the design of the elements based on flexure is sufficient. In the case of the constant depth of beams, the shear strength improved when increasing the (a/d) shear span-to-depth ratio, and the diagonal shear cracks were eliminated. Consequently, on the other hand, when decreasing the (a/d) shear span-to-depth ratio, the propagations of shear diagonal cracks increased beside supports, and the shear strength of the beams decreased. In the case of the load becoming one-point (concentrated load) at mid-span and [shear span (a) = $L/2$], it could be noted that the shear failure will take the strut path, which is a pyramidal diagonal shear crack that starts from the middle point of the beam to the ends of the support.

Fahmy et al. (2014) studied how the type and number of layers of steel mesh affected the way the beams of the U-shaped ferrocement formwork performed. The findings showed that these beams had superior fracture control, high ductility, and improved energy absorption under high ultimate and serviceability loads.

Nassif and Najm (2004) evaluated numerous beam samples with different mesh types (square and hexagonal) using a 2-point loading mechanism until failure. Additionally, they used the ABAQUS application to run a finite element (FE) model. Their findings demonstrated that, in comparison to their experimental findings, the FE model provides accurate results.

Fouad et al. (2020) studied how the two different types of apertures in ferrocement I-beams affected their structural behavior. It is obvious that the strength of beams is diminished with the addition of openings, depending on the location, size, and number of openings. A ferrocement I-beam was made, according to ACMA (2014), by

connecting two ferrocement channel-beams together that are strengthened with 2, 4, and 6 welded wire mesh. The study's results showed that the beam performed well in terms of flexural strength, but it did not exhibit the expected ductility behavior of beams made of reinforced concrete (Acma & Mariano, 2014).

The behavior of reinforced concrete (RC) walls reinforced with various ferrocement composite types under eccentric and concentric loading was examined by Erfan et al. (2021b). The test results indicate that walls with expanded wire mesh exhibited a higher ultimate load than conventionally reinforced control walls by about 105.0% for specimens with two layers of expanded wire mesh without steel stirrups. Specimens reinforced with expanded steel mesh showed a greater strength gain of approximately 111.0% than those reinforced with horizontal steel reinforcement.

El-Sayed et al. (2022) conducted an experimental and analytical study on the flexural performance of HSC beams with a compressive strength of 60 MPa using locally produced hybrid-GFRP (HGFRP) bars and steel wires. The test results show that, when they reach their maximum capacity, H-GFRP bars exhibit the same mechanical failure mechanism as reinforcement steel bars, giving rise to a ductile failure mode. Additionally, the ultimate loads of beams reinforced with H-GFRP bars are higher than those of beams reinforced with steel and regular GFRB bars.

A type of ferrocement that Abdullah and Abdulla (2022) examined was a hollow ferrocement beam of self-compacting mortar reinforced with different kinds of non-metallic (GFRP bars, fiber glass mesh) and metallic (steel bars) reinforcement. The findings demonstrated that the loads were greater by 7.51%, 9.88%, and 5.15%, respectively, for hollow ferrocement beams reinforced with GFRP bars and several layers of fiber glass mesh (one, two, and three).

El-Sayed et al. (2023b) performed an experimental and mathematical investigation into the behavior of ferrocement composite tanks under static pressure loads. The experimental results indicate that ferrocement composite tanks' failure load is higher than conventionally reinforced concrete tanks, particularly those reinforced with fiberglass polymer mesh.

The effectiveness of ferrocement pipes reinforced with various metallic and non-metallic materials was examined by El-Sayed et al. (2023a). The findings demonstrated that the failure load of ferrocement pipes is higher than that of traditional concrete pipes. Among the other versions with the lowest failure load (strength), the pipes reinforced with a combination of welded and expanded wire meshes are the most expensive.

El-Sayed (2021) investigated the composition and characteristics of ferrocement geopolymer HSC columns made with rice straw ash (RSA) and subjected them to axial loading. The findings demonstrated that early cracks, ultimate loads, energy absorption, and ductility index increased with a rise in the wire mesh reinforcement's volume fraction. The ultimate load, ductility, and energy absorption of ferrocement geopolymer columns were higher than those of the steel-reinforced concrete control column.

Al-Sulaimani et al. (1991) used 15 beam specimens to perform flexural testing to investigate the shear behavior of ferrocement box beams. According to test results, increasing the amount of wire mesh in webs increases cracking and ultimate shear pressures; adding wire mesh to flanges, on the other hand, increases shear resistance by stopping tension cracks and making them finer.

An experimental and numerical study is being done on the flexure behavior of geopolymer ferrocement beams under axial flexural stress, as investigated by El-Sayed et al. (2023c). According to test results, the ultimate loads of the specimens tested with ferrocement were approximately 15% lower than those of the control group. As the volume percent of the wire mesh reinforcement rose, the ductility index, ultimate loads, energy absorption, and initial fractures all improved.

On the other hand, many studies have been done on the structural behavior of RC elements reinforced by ferrocement. Erfan et al. (2019a) studied the structural performance of eccentric ferrocement-reinforced concrete columns. Erfan et al. (2019b) conducted an experimental and analytical behavior of HSC columns reinforced with basalt FRP bars. Abdallah et al. (2019) conducted an experimental and analytical analysis of lightweight ferrocement composite slabs. Erfan et al. (2021a) studied the flexural behavior of HSC one-way slabs reinforced with basalt FRP bars. Adam et al. (2021) studied the

Table 1 Geometric and physical properties of the steel mesh

Mesh type	Mesh entry (mm)		Dim. of strands (mm)		Diameter (mm)	Grid size (mm)	Weight (gm/m ²)	Proof stress (MPa)
	Long	Short	Width	Thickness				
WWM	–	–	–	–	0.8	12.5 × 12.5	320	400
EMM	35	18	2	1			630	199

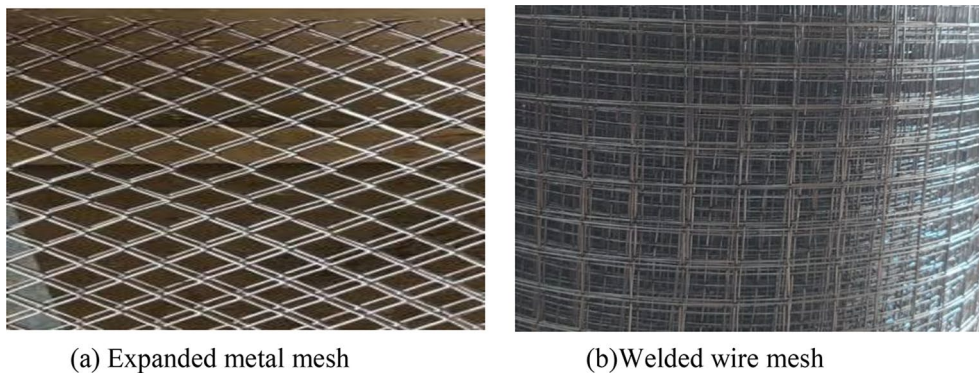


Fig. 1 Various mesh types used for reinforcing

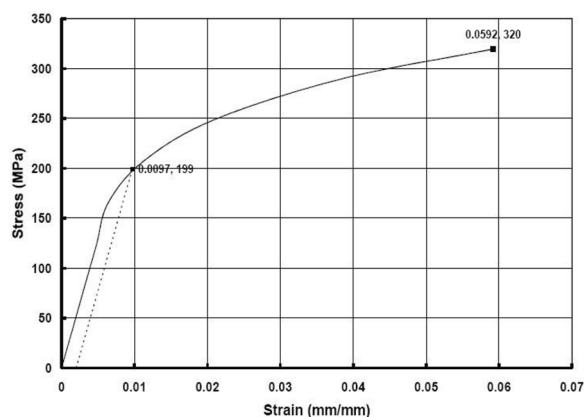


Fig. 2 Stress-strain relationship for the expanded wire mesh

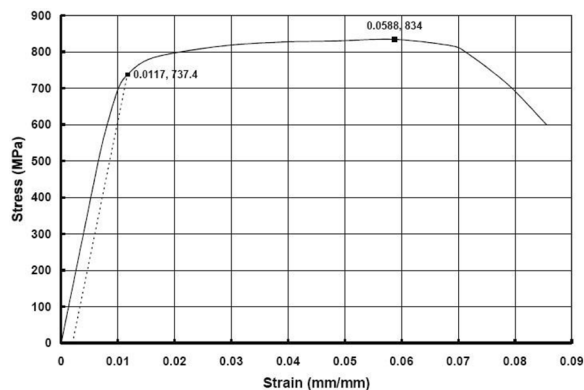


Fig. 3 Stress-strain relationship for the welded wire mesh

structural behavior of high-strength concrete slabs reinforced with GFRP bars. Nassif et. al. (2021) studied the flexural behavior of high-strength concrete deep beams reinforced with GFRP bars. Erfan and El-Sayed (2019a) studied the structural shear behavior of composite box beams using advanced innovative materials. Abdullah

and Abdulla (2023) investigated the flexural behavior of box ferrocement beams consisting of self-compacted mortar reinforced by fiber glass mesh and GFRP bars after exposure to high temperatures. El-Sayed and Algash (2021) studied the flexural behavior of ultra-high-performance geopolymer RC beams reinforced with GFRP bars.

2 Research Signification

The main objective of this study is to study the behavior of lightweight reinforced concrete beams reinforced with various metal mesh reinforcement materials as a potential replacement for conventional reinforced concrete beams. Two types of steel mesh are employed in different layers to reinforce those low-weight beams: expanded steel wire mesh and welded wire mesh. The recommended beams weigh less than standard reinforced concrete beams. The kind of steel reinforcement used, the number of layers of steel reinforcement employed, and the type of concrete used were all examined in this study. To confirm the outcomes of the experimental program, ABAQUS, a finite element tool, will perform a theoretical analysis.

3 Experimental Program

The experimental program was implemented in the Benha Faculty of Engineering laboratory at Benha University, Egypt. The primary aim of the study was to examine the shear behavior of reactive powder concrete ferrocement specimens reinforced with expanded wire mesh and welded wire mesh, and with different light weight core materials, in comparison with the control specimens made from concrete and reactive powder concrete. The first crack, deflection, ultimate load, crack pattern, and ductility index were determined for each specimen, and the mode of failure at collapse was observed.

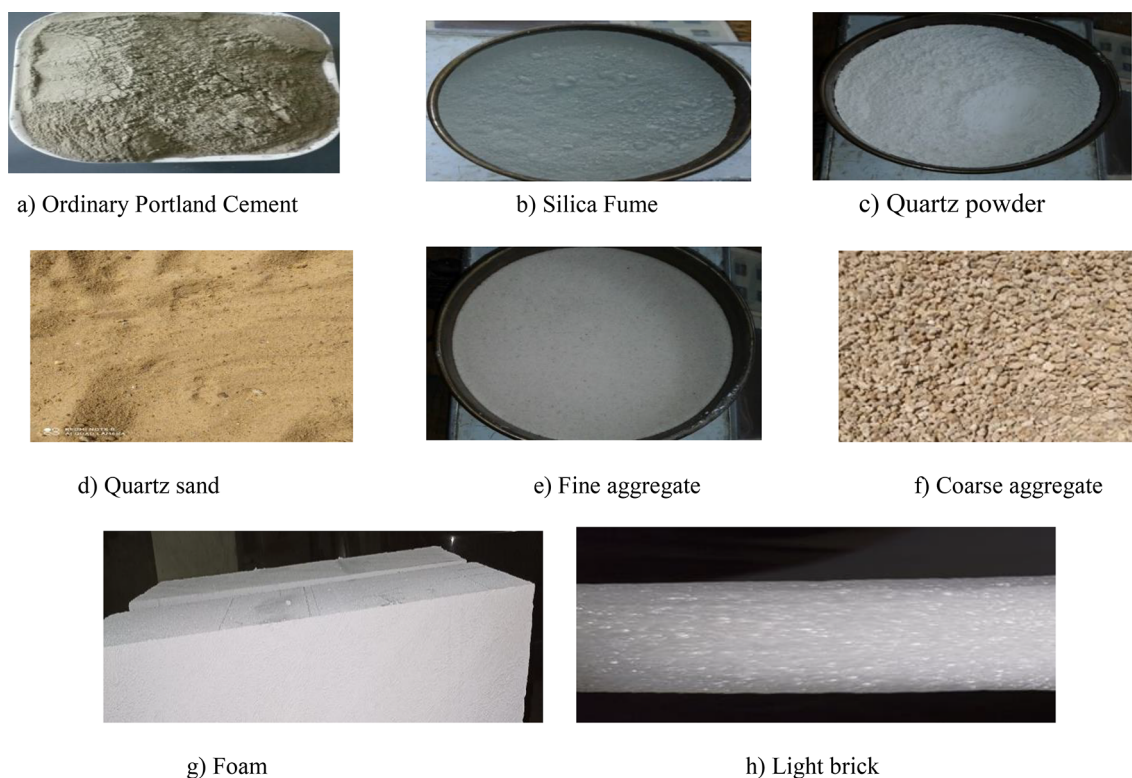


Fig. 4 The material used to produce the normal concrete and ferrocement mortar

Table 2 Percentages by weight of a typical concrete mix

Material	Cement	Coarse aggregate	Fine aggregate	Water	Superplasticizer
Weight (kg/m ³)	560	1090	586	168	6

The materials used are:

Fine aggregate: The sand was siliceous naturally. Its qualities meet the requirements of ASTM C136-84a. It had a specific gravity of 2.67 and a fineness modulus of 2.55, making it clear and almost impure free (ASTM C778, 2021)

Coarse aggregate: With a specific gravity of 2.76, a crushing modulus of 18.5%, and water absorption of 2.1%, the crushed dolomite met the standards of Egyptian Code 203/2007. These particles had a relatively low fraction of flat particles and were asym-

metrical and angular in shape (Egyptian Standards Specification, 2012)

Quartz sand: The quartz sand utilized in this study has a specific gravity of 2.65, with particle sizes ranging from 1.18 to 2.36 mm.

Quartz powder: The quartz powder, with a mean particle size of 10–15 μm, employed in this study was produced locally in Egypt.

Cement: Type I Portland cement complied with ASTM C/150-07 and was ordinary Portland cement of grade 42.5N (ASTM C/150-07, 2007).

Silica fume (S.F): It increases the strength of normal concrete and ferrocement mortar. It was employed in mortar formulations as a weight-for-weight partial replacement for cement imported from the Sika company in Egypt.

Water: It was safe for drinking, devoid of contaminants that would compromise the strength, and ideal for mixing concrete, concrete strength, and durability.

Table 3 Percentages by weight of ferrocement mortar mix

Material	Cement	Silica fume	Quartz sand	Quartz powder	Water	Superplasticizer
Weight (kg/m ³)	560	235	885	220	200	6

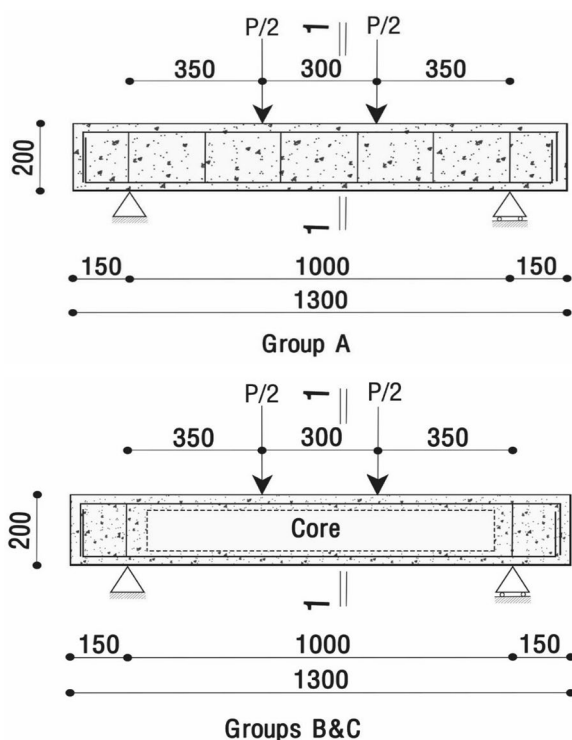


Fig. 5 Typical dimensions and reinforcement of the tested specimens (all measurements are in mm)

Superplasticizer: It has a 1.21 kg/l density at room temperature and complies with ASTM C 494/C494M (2005). Two dosages of the superplasticizer were employed. In Egypt, Visco Crete 1000 RM from the Sika Company has been used at the recommended dose of 0.15–0.30% of cement weight (or roughly 0.6 kg/m³ of concrete) for greater workability without water reduction.

Reinforcing steel: High-tensile deformed bars with a nominal yield strength of 360 N/mm² were used as the longitudinal steel reinforcement in all specimens. Mild steel stirrups provided shear reinforcement for the control beams with a nominal yield strength of 240 N/mm² and a diameter of 6 mm.

Mesh reinforcement: Expanded metal mesh (EMM) and square welded wire steel mesh (WWM), both readily accessible in local markets, reinforce the ferrocement beams. Table 1 provides information about the mesh's characteristics. In Fig. 1, the steel meshes are shown from a photographic perspective. Figs. 2 and 3 illustrate the stress–strain relationship for the expanded steel mesh and welded wire mesh, respectively.

Extruded foam core (EFC): It served as the foundation material for group B specimens. It is a white-

board (2 by 1 m) made using a continuous extrusion method with special qualities like low heat conductivity, excellent water resistance, high compressive strength, and a 38 kg/m³ density.

Autoclaved aerated lightweight brick core (AAC): It served as the primary component of group C specimens. It is a brick that was manufactured commercially and measures 60×20×10 cm. According to the technical information that has been made publicly available, this sort of brick has a dry unit weight of 600–640 kg/m³, a porosity of 20–28%, and a thermal conductivity (K) of 0.26–0.32 W/m°C. Figure 4 shows the materials used.

3.1 Matrix of Concrete and Mortar

The mix ratios by weight per cubic meter for the usual weight concrete used as a specimen, A1, are presented in Table 2. Reactive powder concrete, used for specimen A2 and specimens of group B&C (ferrocement beams), was constructed using mortar that met the requirements of ACI 549.1R-88 and ACI 549-1R-93 (1999). The mix proportions are presented in Table 3.

A sufficient amount of superplasticizer was added to make mortar mixes more workable. Three cubes, each measuring 70×70×70 mm, were cast for the conventional concrete mix and the ferrocement mortar mix to test the strength of the mixtures. For normal concrete, the compressive strength is 54.73 MPa after 28 days. The compressive strength of the mortar used to prepare the ferrocement beams is 64.4 MPa after 28 days.

3.2 Samples Description

The experimental program consists of ten composite beams with simple support and the same dimensions of 100×200×1300 mm. The specimens were tested under two point-load loads with a 350 mm shear span and a 300 mm load distance. The specimens were divided into three groups (A, B, and C). The beams of group A (control beams): A1 was cast with a normal concrete beam, while A2 was cast with a reactive powder concrete beam. EFC, a reinforced extruded foam core, was used to make the beams for Group B. Beams of Group C were made of reinforced autoclaved aerated lightweight brick core (AAC). Fig. 5 shows the typical dimensions and reinforcement of the tested samples. The cross-sectional features of the beams are shown in Fig. 6. Table 4 summarizes the details of the test specimens.

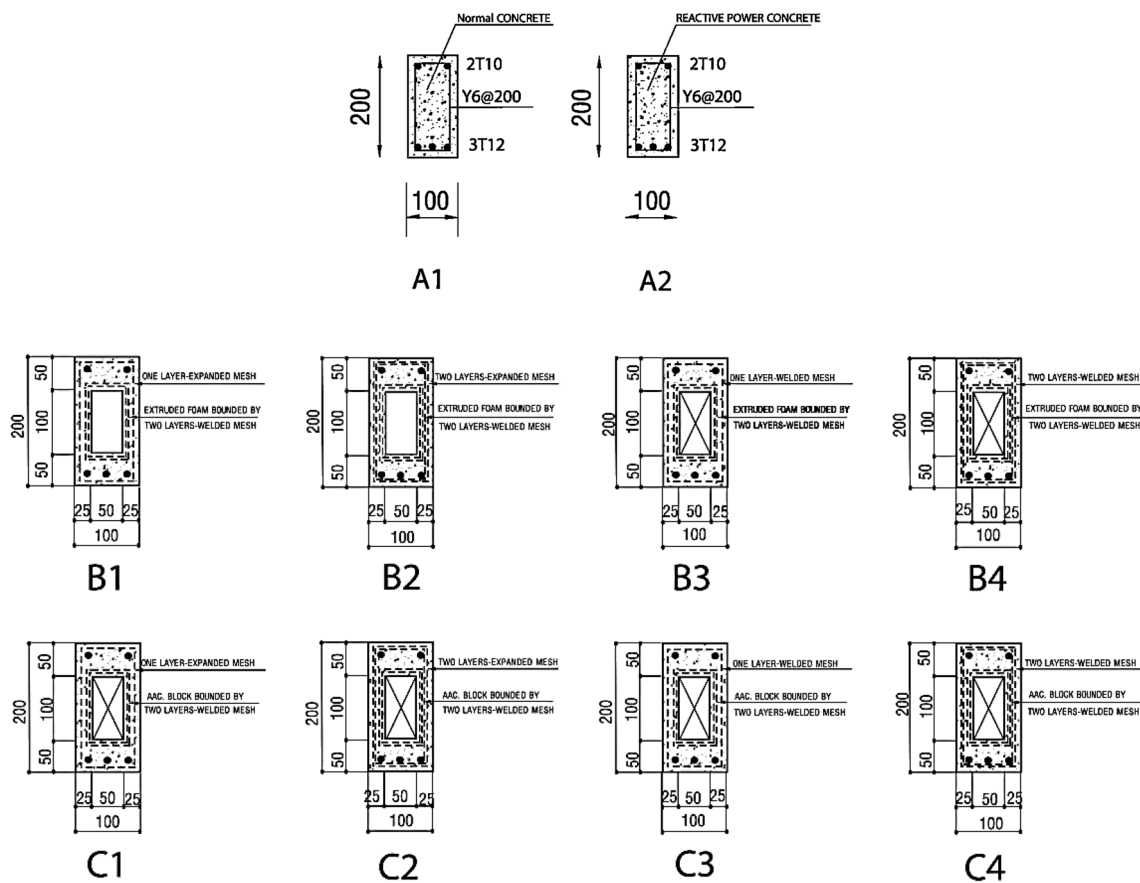


Fig. 6 Typical cross-sections of tested specimens

Table 4 Specifics of the beams

Group	Specimen name	Specimen's core type	Links	No. of layers	Type of mesh	Concrete type
A	A1	–	5 ϕ 6/m	–	–	Normal concrete
	A2	–	5 ϕ 6/m	–	–	Reactive powder concrete
B	B1	EFC	–	1	EMM	Reactive powder concrete
	B2	EFC	–	2	EMM	Reactive powder concrete
	B3	EFC	–	1	WWM	Reactive powder concrete
	B4	EFC	–	2	WWM	Reactive powder concrete
C	C1	AAC	–	1	EMM	Reactive powder concrete
	C2	AAC	–	2	EMM	Reactive powder concrete
	C3	AAC	–	1	WWM	Reactive powder concrete
	C4	AAC	–	2	WWM	Reactive powder concrete

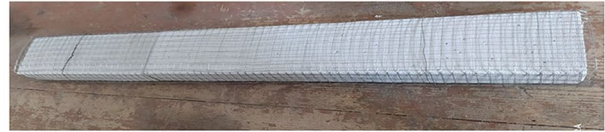
3.3 Preparation of Test Specimen

The specimens were cast using a wooden form that was designed to cast two pieces simultaneously. Fig. 7 depicts the form, the primary wire mesh caging, the ferrocement cores wrapped in WWM and EMM, and the demolded beam. After the wooden mold was put together, the beams

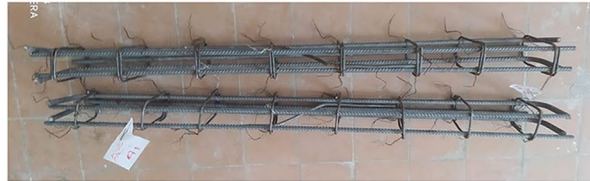
were cast, a thin layer of shuttering oil was applied, and reinforcing caging was added. To adequately cover the steel wire mesh for the ferrocement beams, spacers were pressed into the mortar layer after the mortar had been poured and vibrated in the mold to a thickness of fifty millimeters. After the caging was set in place, the concrete for



a) Wooden form assembly.



i) Light Bricks Bounded by Two Layers of Welded Wire Mesh.



b) Reinforcement of Control Specimens (A1 and A2).



j) One Layer of Expanded Metal Mesh (C1).



c) Foam Bounded by Two Layers of Welded Wire Mesh.



k) Two Layers of Expanded Metal Mesh (C2).



d) One Layer of Expanded Wire Mesh (B1).



l) one Layer of Welded Wire Mesh (C3).



e) Two Layers of Expanded Wire Mesh (B2).



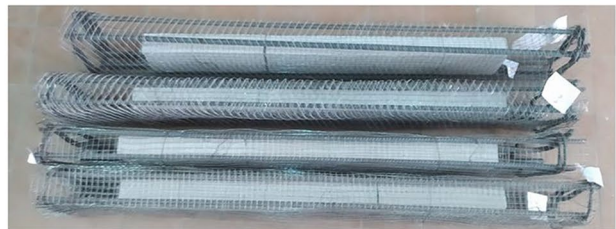
m) Two Layers of Welded Wire Mesh (C4).



f) One Layer of Welded Wire Mesh (B3).



g) Two Layers of Welded Wire Mesh (B4).



n) Reinforcement of Group Number (C).



h) Reinforcement of Group Number (B).



Fig. 7 Steps of specimen preparation



p) Molded beams.

Fig. 7 continued

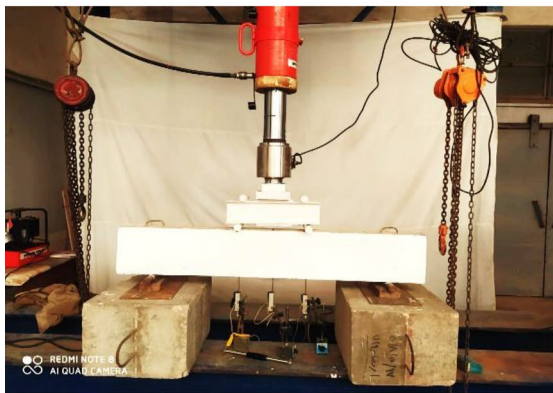


Fig. 8 Test setup

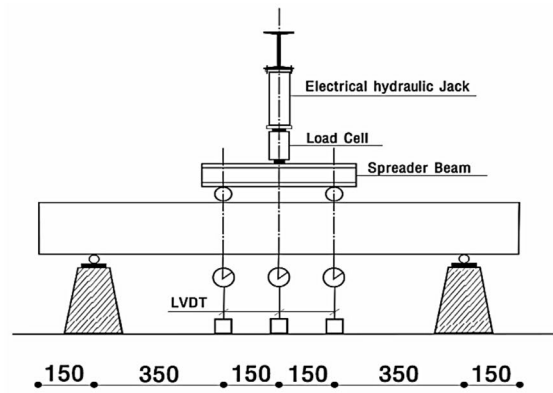


Table 5 Experimental results

Group	Specimens designation	F.C.L, kN	Ult. load, kN	Def. at F.C.L, mm	Def. at Ult. load, mm	Ductility index
A	A1	24.93	105.22	1.32	6.91	5.25
	A2	28.29	112.82	1.26	6.66	5.27
B	B1-1E	32.08	116.48	1.59	7.79	4.91
	B2-2E	33.87	125.98	1.64	7.97	4.87
	B3-1W	27.08	108.2	1.06	6.87	6.45
	B4-2W	28.99	113.13	1.37	7.79	5.70
C	C1-1E	32.94	119.97	1.28	7.62	5.96
	C2-2E	34.57	129.53	1.28	8.18	6.37
	C3-1W	29.98	111.8	1.20	7.13	5.95
	C4-2W	31.05	115.59	1.38	7.91	5.72

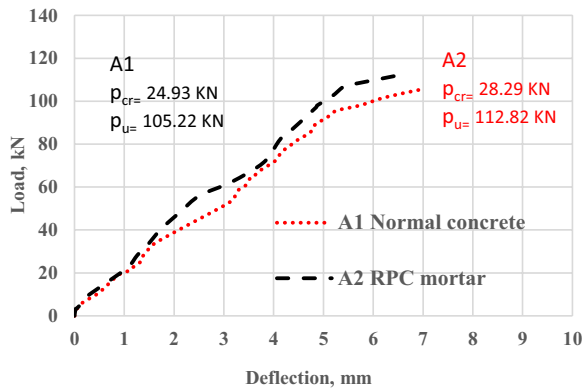


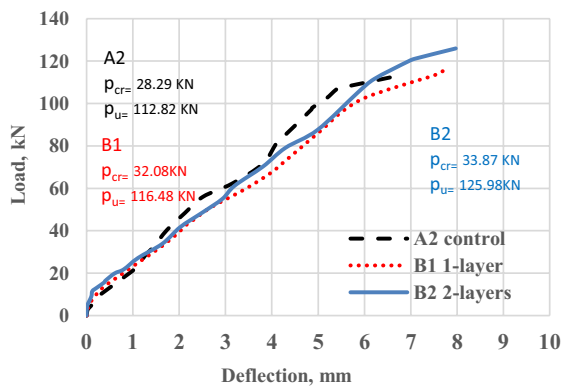
Fig. 9 Load–deflection curves for specimens of group (A)

the control beams or the mortar matrix for the ferrocement beams was poured and vibrated using an electrical vibrator

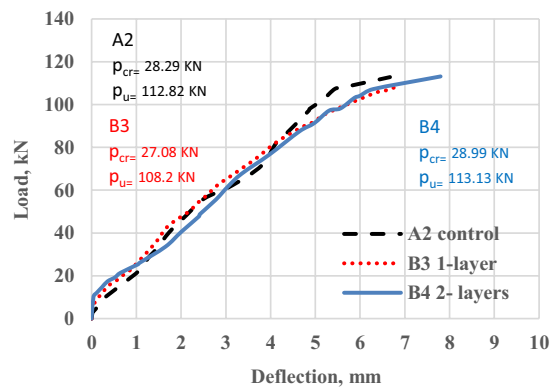
to guarantee adequate compaction and to get rid of any air gaps. Before disassembling the form, the ferrocement forms were left for 24 h. All the previous steps are shown in Fig. 7.

3.4 Test Setup

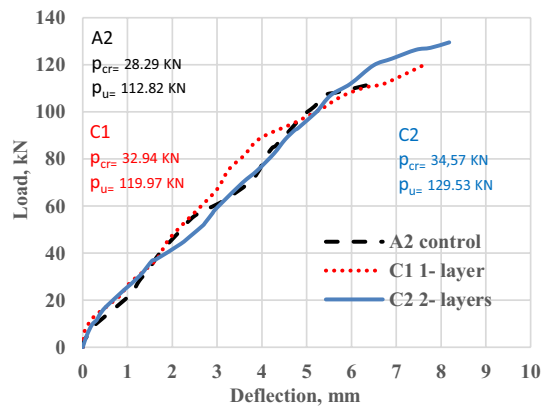
The beam specimens were tested under a two-point load testing machine with a maximum capacity of 200 kN, a 1000 mm effective span, a 350 mm shear span, and a 300 mm load distance, as shown in Fig. 8. The load was applied in increments of 5 kN to the tested specimens. To track deflection at the point of load application, a linear variable displacement transducer (LVDT) was positioned at the midpoint of the test beam, as shown in Fig. 8. To clearly see the crack patterns, white emulsion was used to paint the beams. The test was initiated by correctly positioning the specimens in the loading frame. A tiny load was first applied to ensure that every instrument was functioning.



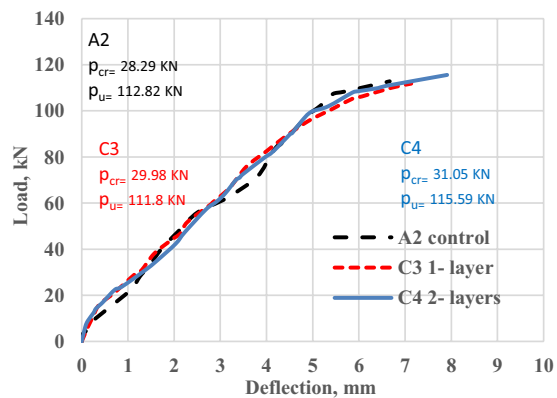
(a) Load-Deflection curves for specimens B1 & B2 (with EMM & EFC), and A2.



(b) Load-Deflection curves for specimens B3 & B4 (with WWM & EFC), and A2.

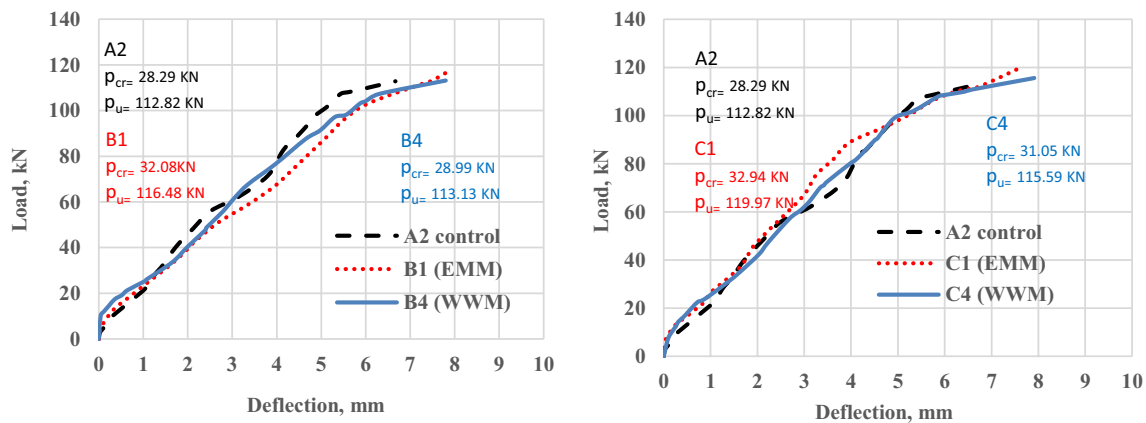


(c) Load-Deflection curves for specimens C1 & C2 (with EMM & AAC), and A2.



(d) Load-Deflection curves for specimens C3 & C4 (with WWM & AAC), and A2.

Fig. 10 The effect of the number of steel mesh layers on the load–deflection



(a) Load-Deflection curves of specimens B1, B4 and A2.

(b) Load-Deflection curves of specimens C1, C4 and A2.

Fig. 11 The effect of steel mesh type on the load–deflection curves

The force was then steadily raised until the specimen failed. When excessive cracking developed at the beam's shear span, the ultimate load was calculated. Where the applied load decreased, and deflection increased. The ultimate load was automatically recorded at each load increment using a computerized data acquisition (DAQ) system.

4 Experimental Results and Discussions

The investigated structural attributes comprised crack pattern, ductility index, failure mode, first crack load, ultimate load, deflection at the first crack load, and deflection at the ultimate load. The load–deflection curves of the examined specimens were also drawn. The deflection at first fracture load, also known as the deflection at first crack commencement, on the curve represents the point at which the curve deviates from the initial linear connection. The ductility index measures how much a material deflects under ultimate stresses relative to its deflection at the first crack. A beam has more warnings before ultimately collapsing if its ductility index value is higher. The aforementioned values are listed in Table 5.

4.1 Load–Deflection Relationships

Generally, all ferrocement specimens with lightweight core material had higher resistance than the control specimens A1 (normal concrete) and A2 (reactive powder concrete), according to the research done by Shaaban et al. (2018b). The ultimate loads and maximum deflection of ferrocement specimens with lightweight core material are higher than the corresponding values of normal concrete specimens (A1) by a range of 2.8% to 18.8% for the ultimate load and by a range of 10.3% to 15.6% for

the maximum deflection. Also, the ultimate loads of ferrocement specimens with light weight core material are higher than the corresponding values of reactive powder concrete specimen (A2), except specimens (B3–1W) and (C3–1W).

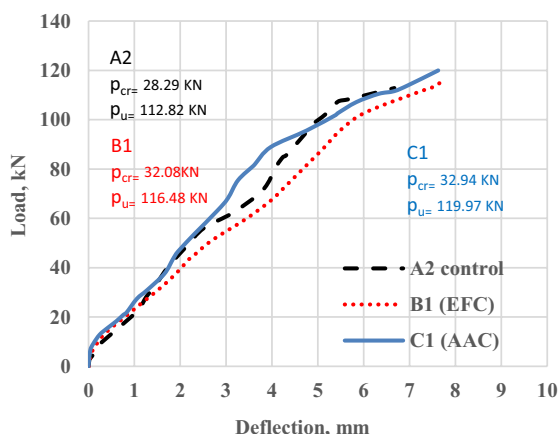
The specimen (C2–2E) revealed the highest ultimate load and maximum deflection values by 14.8% and 18.6%, respectively, compared to specimen A2. The next sections explain the load–deflection relationship of the tested specimens.

4.1.1 Effect of the Concrete Type

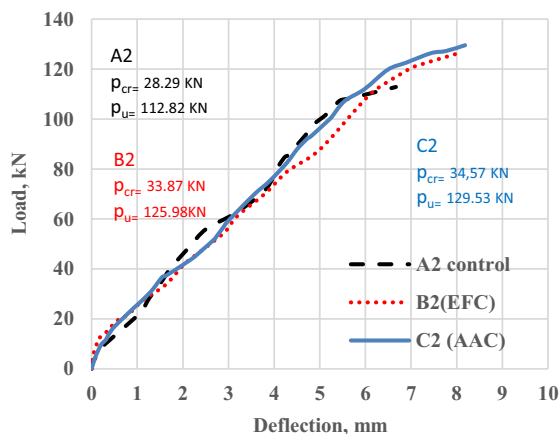
The comparison between the load–deflection relationships of the two specimens (A1 and A2) didn't show a significant difference in behavior. Fig. 9 shows the load–deflection curves of the control specimen for the normal concrete beam (A1) and the beam with reactive powder concrete (A2). The ultimate load of specimen A1 is less than that of specimen A2 by about 7.2%. Also, deflection at the maximum load of specimen (A1) increased by 3.8% compared to specimen (A2). This is due to the different types of concrete, which was agreed with Shaaban et al. (2018a).

4.1.2 The Effect of the Number of Steel Mesh Layers

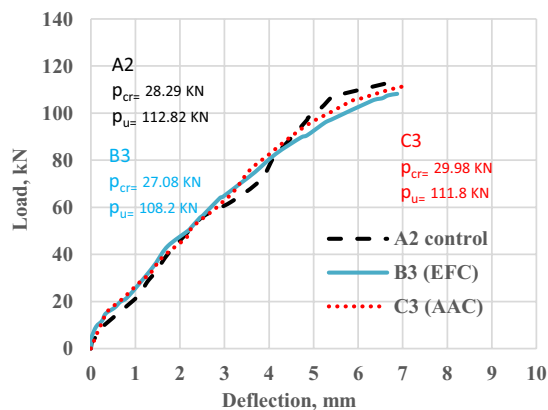
It was clear from the laboratory results that when using two layers of steel mesh, there was a higher ultimate load and maximum deflection. Fig. 10a, b illustrate the load–deflection curves for the specimens in group B, with EFC core material reinforced by EMM and WWM, respectively. Also, the corresponding curve for control specimen A2 is presented for comparison.



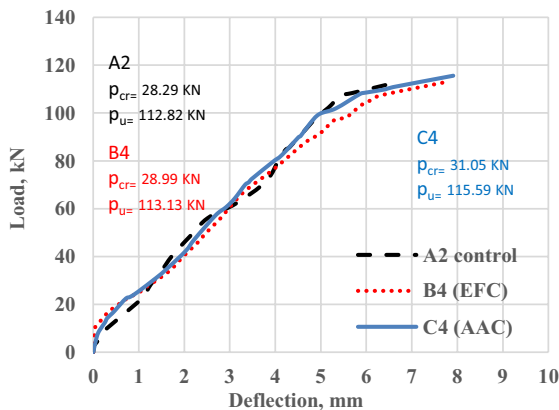
(a) Load-Deflection curves due to type of core for (B1&C1) compared to A



(b) Load-Deflection curves due to type of core for (B2&C2) compared to A2.



(c) Load-Deflection curves due to type of core for (B3&C3) compared to A2.



(d) Load-Deflection curves due to type of core for (B4&C4) compared to A2.

Fig. 12 The effect of core material type on the load–deflection curves

Table 6 The number of cracks and the width at the ultimate load crack for each sample

Sample	Number of cracks	Crack width at ultimate load (mm)
A1	11	0.855
A2	11	2.062
B1–1E	12	2.055
B2–2E	15	1.533
B3–1W	12	0.737
B4–2W	11	1.153
C1–1E	12	3.095
C2–2E	13	1.19
C3–1W	10	2.247
C4–2W	11	2.16

Increasing the number of layers of EMM from one layer (specimen B1) to two layers (specimen B2) led to an increase in the ultimate load and maximum deflection by 8.15% and 2.31%, respectively. The ultimate load and maximum deflection of specimen B2 were increased by 11.6% and 19.66%, respectively, compared with the control specimen A2, as shown in Fig. 10a.

Increasing the number of layers of WWM from one layer (specimen B3) to two layers (specimen B4) led to an increase in the ultimate load and maximum deflection by 4.4% and 11.8%, respectively. The ultimate load and maximum deflection of specimen B4 increased by 2.1% and 14.5%, respectively, compared with the control specimen A2, as shown in Fig. 10b.

Fig. 10c, d illustrate the load–deflection curves for the specimens of group C, with AAC core material reinforced by EMM and WWM, respectively. Also, the

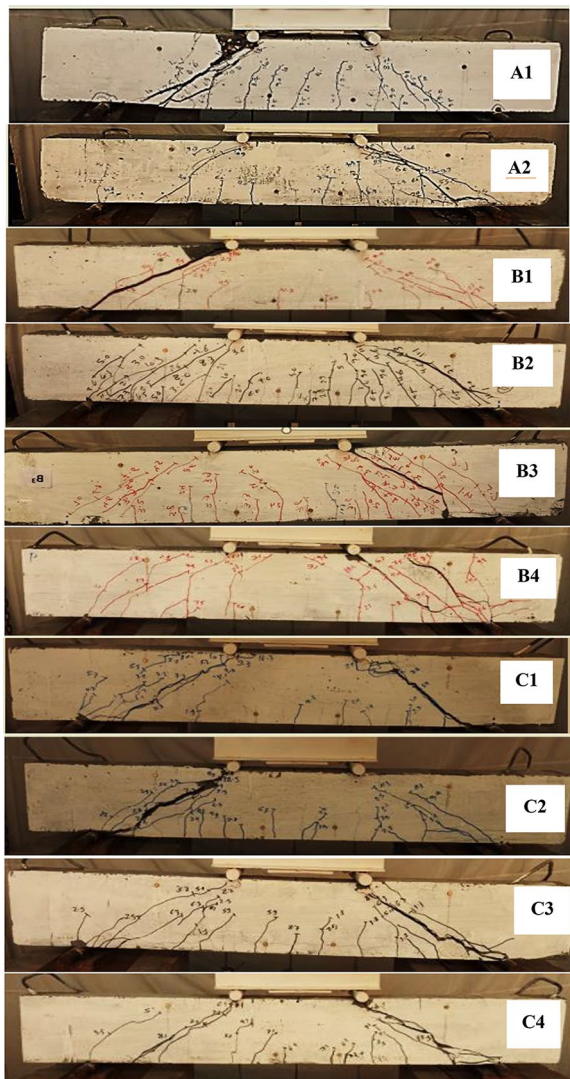


Fig. 13 Cracking patterns of tested beams

corresponding curve for control specimen A2 is presented for comparison.

Increasing the number of layers of EMM from one layer (specimen C1) to two layers (specimen C2) led to an increase in the ultimate load and maximum deflection by 7.3% and 6.8%, respectively. The ultimate load and maximum deflection of specimen C2 were increased by 12.9% and 18.5%, respectively, compared with the control specimen A2, as shown in Fig. 10c.

Increasing the number of layers of WWM from one layer (specimen C3) to two layers (specimen C4) led to an increase in the ultimate load and maximum deflection by 3.2% and 10.9%, respectively. The ultimate load and maximum deflection of specimen C4 were increased by 2.4% and 15.8%, respectively, compared with the control

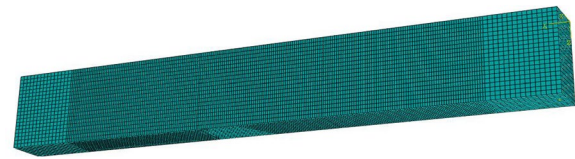


Fig. 14 Model of the analyzed beams by NLFEA

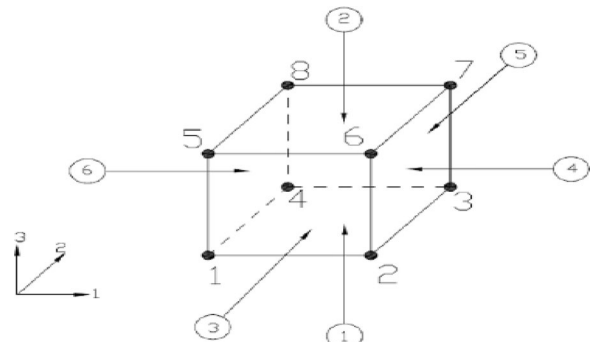


Fig. 15. 3-Dimensional solid (brick) element

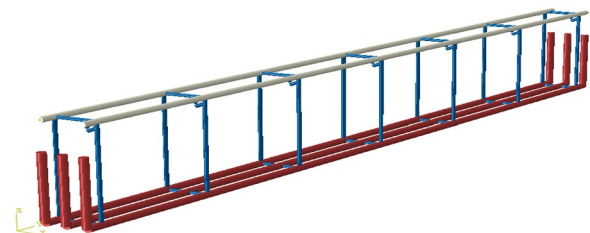


Fig. 16 Truss element modeling for steel bar reinforcement

specimen A2, as shown in Fig. 10d. These results are consistent with the Erfan and El-Sayed research (Erfan & El-Sayed, 2019b).

4.1.3 The Effect of Steel Mesh Type

Fig. 11a, b illustrates the impact of the steel mesh type (EMM and WWM) on the load–deflection curve. The load–deflection curve of control specimen A2 was also presented for comparison.

Fig. 11a presents the steel mesh type’s impact for specimens B1 and B4, which have the same light core material (EFC) and also have a similar reinforcement area where one layer of EMM (specimen B1) is approximately equivalent to two layers of WWM (specimen B4).

Using one layer of EMM (specimen B1) was better than using two layers of WWM (specimen B4), which led to

an increase in the ultimate load of 2.9% but the same maximum deflection. The ultimate load and maximum deflection of specimen B1 were increased by 3.14% and 14.5%, respectively, compared with the control specimen A2, as shown in Fig. 11a.

Fig. 11b presents the effect of the steel mesh type on specimens C1 and C4, which have the same light core material (AAC) and also a similar reinforcement area where one layer of EMM (specimen C1) is approximately equivalent to two layers of WWM (specimen C4).

Using one layer of EMM (specimen C1) was better than using two layers of WWM (specimen C4), which led to an increase in the ultimate load by 3.7% but less than that in maximum deflection by 3.6%. The ultimate load and maximum deflection of specimen C1 were increased by 6% and 12.6%, respectively, compared with the control specimen A2, as shown in Fig. 11b. These results are consistent with the results of Shaaban et al. research (Shaaban et al., 2018a).

4.1.4 The Effect of Core Material Type

According to the experimental results, the effect of core material type was nonsignificant for all tested specimens. For specimens reinforced by one layer of EMM (specimens B1 and C1), using AAC as a core material (specimen C1) instead of EFC (specimen B1) increased the ultimate load and maximum deflection by 3% and 2.3%, respectively, as shown in Fig. 12a.

For specimens reinforced by two layers of EMM (specimens B2 and C2), using AAC as a core material (specimen C2) instead of EFC (specimen B2) leads to an increase in the ultimate load and the maximum deflection by 2.9% and 2.6%, respectively, as shown in Fig. 12b. For specimens reinforced by one layer of WWM (specimens B3 and C3), using AAC as a core material (specimen C3) instead of EFC (specimen B3) leads to an increase in

the ultimate load and the maximum deflection by 3.3% and 3.8%, respectively, as shown in Fig. 12c. For specimens reinforced by two layers of WWM (specimens B4 and C4), using AAC as a core material (specimen C4) instead of EFC (specimen B4) leads to an increase in the ultimate load and the maximum deflection by 2.2% and 1.5%, respectively, as shown in Fig. 12d. These results are consistent with the results of Shaaban et al. research (Shaaban et al., 2018a).

4.2 Crack Patterns

All tested specimens failed due to diagonal tensile stresses produced by shearing forces, where a wide diagonal crack within the shear span was propagated at the ultimate load.

Table 6 shows the number of cracks and the width of each crack at the ultimate load for each sample. Fig. 13 shows the cracking patterns for groups A, B, and C specimens, respectively. Firstly, vertical cracks (flexural cracks) due to tensile stresses were observed in the mid-span region. The first crack in the control specimens (A1 and A2) was observed at a load of 35 kN and 34 kN, respectively, while the first crack in group B was observed at 24 kN, 2 kN, 24 kN, and 21 kN for specimens B1, B2, B3, and B4, respectively, while the first crack in group C was observed at 19 kN, 22 kN, 25 kN, and 20 kN for specimens C1, C2, C3, and C4, respectively. Due to the same process, cracks appear for other samples. For tested beams, using welded wire mesh and expanded wire mesh in place of stirrups improves the crack pattern. The final flexural crack, which inclined and crossed mid-depth in the shear span zone, was followed abruptly by the diagonal crack that caused the collapse. The crack then continued to spread along the tensile reinforcement in both

Table 7 Finite element analysis results

Group	Specimens designation	F.C.L, kN	Ult. I, kN	Def. at f.c.l, mm	Def. at ultimate load, mm	Ductility index
A	A1	25.16	110.36	0.92	6.25	6.82
	A2	27.56	120.84	0.95	6.40	6.75
B	B1-1E	31.11	124.43	1.05	8.17	7.81
	B2-2E	32.20	128.78	0.97	8.26	8.50
	B3-1W	27.82	111.27	0.99	7.32	7.37
	B4-2W	30.29	121.15	1.05	7.77	7.41
C	C1-1E	31.60	126.40	1.03	8.06	7.85
	C2-2E	33.28	133.11	0.96	7.97	8.32
	C3-1W	29.67	118.64	0.99	7.20	7.26
	C4-2W	30.92	123.66	1.02	7.44	7.32

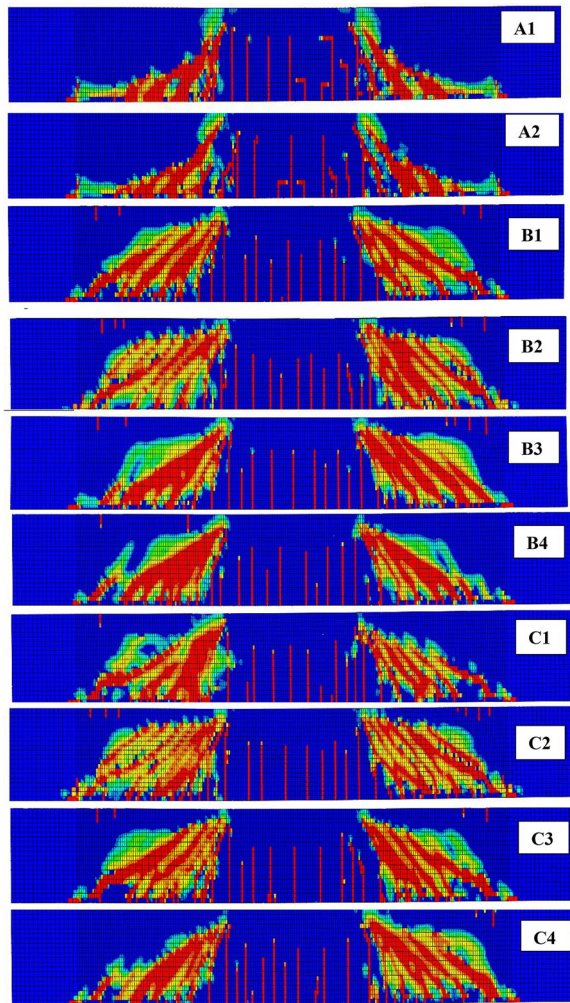


Fig. 17 Cracking patterns for finite element models

directions (due to the action of the dowel), causing the bond to break and the beam to fail. Generally, using ferrocement led to better crack distribution, where a greater number of narrow cracks were observed, especially in specimens reinforced by two layers of steel mesh.

5 Finite Element Modeling

All the specimens were modeled and analyzed using the ABAQUS/CAE program (Abaqus, 2013). The validity of the created finite element models was assessed using the experimental data.

5.1 Specimens Modeling

The behavior of the composite beams made of ferrocement depicted in Fig. 14 was estimated using nonlinear finite element analysis (NLFEA). The ultimate capacity, deflection, and fracture distribution of each specimen were all discussed behaviors.

5.2 Elements' Description

5.2.1 Solid Element

Concrete beams were modeled using the C3D8R, or brick element, shown in Fig. 15. The element's nodes each have three degrees of freedom that are in between states. This component was chosen because it can specify the limits of the RC plate property and the contact faces required to apply loading. Furthermore, it closely adheres to constitutive law integration, is very well suited for dynamic analysis, nonlinear statics, and rotation, and permits finite strain in large-displacement studies. The C3D8R element was used to represent the impactor as well.

Table 8 Comparison between experimental and NLFEM analysis

Sample ID	EXP				NLFEM				Pult, FEM/ Pult, EXP
	1st crack load (kN)	Def. at 1st crack load, (mm)	Ult. L (kN)	Ult. Def. (mm)	1st crack load (kN)	Def. at 1st crack load, (mm)	Ult. L (kN)	Ult. Def. (mm)	
A1	24.93	1.32	105.22	6.91	25.16	0.92	110.36	6.25	1.05
A2	28.29	1.26	112.82	6.66	27.56	0.95	120.84	6.40	1.07
B1-1E	32.08	1.59	116.48	7.79	31.11	1.05	124.43	8.17	1.07
B2-2E	33.87	1.64	125.98	7.97	32.20	0.97	128.78	8.26	1.02
B3-1W	27.08	1.06	108.2	6.87	27.82	0.99	111.27	7.32	1.03
B4-2W	28.99	1.37	113.13	7.79	30.29	1.05	121.15	7.77	1.07
C1-1E	32.94	1.28	119.97	7.62	31.60	1.03	126.40	8.06	1.05
C2-2E	34.57	1.28	129.53	8.18	33.28	0.96	133.11	7.97	1.03
C3-1W	29.98	1.20	111.8	7.13	29.67	0.99	118.64	7.20	1.06
C4-2W	31.05	1.38	115.59	7.91	30.92	1.02	123.66	7.44	1.07



Fig. 18 Comparison between Exp. ultimate load and NLFE ultimate load

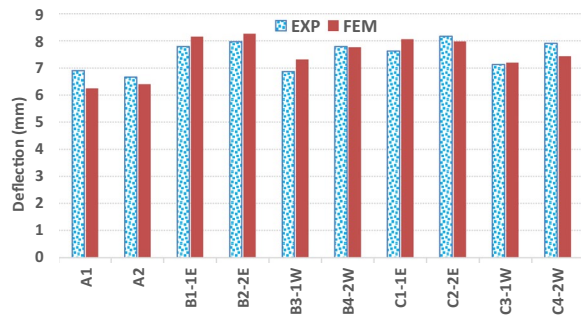


Fig.19 Comparison between Exp. deflection and NLFE deflection

5.2.2 Truss Element

Truss elements are rods that can carry only tensile or compressive forces. They have no resistance to bending; therefore, they are useful for modeling reinforcement within other elements. (T3D2) element was selected in modeling reinforcement bars (see Fig. 16), which were created as components embedded in concrete blocks.

5.3 Material Properties

This paragraph displays the material characteristics of the reinforcing expanded and welded wire mesh, reinforcing steel bars, and concrete.

- Concrete’s material characteristics constants are entered as follows:

The elasticity of the elastic modulus ($E_c = 4400\sqrt{f_{cu}} = 24,100 \text{ N/mm}^2$) and ratio of Poisson ($\mu = 0.3$) (E.C.P.203, 2020).

- These additional material characteristics for steel reinforcement are entered as follows:

1. $E_s = 200 \text{ kN/mm}^2$ is the elastic modulus.
2. Yield stress is 360 N/mm^2 .
3. Ratio of Poisson ($\mu = 0.2$).
4. Steel area of $3\phi 12$ ($A_s = 339.29 \text{ mm}^2$).
5. Steel area of $2\phi 10$ ($A_s = 157.07 \text{ mm}^2$).

- Following are the inputs for the expanded wire mesh’s material properties:

1. Proof stress = 199 N/mm^2 .
2. The diamond has dimensions of $18 \times 35 \text{ mm}$ and a 1.25 mm thickness.
3. One expanded mesh layer’s volumetric ratio ($V = 0.0092$).
4. Two expanded mesh layer’s volumetric ratio ($V = 0.0184$).

- For welded wire mesh, the following material parameters are input:

1. Proof stress = 400 N/mm^2 .
2. With wires that are 0.08 cm in diameter, the opening is $1.25 \times 1.25 \text{ cm}$ in size.
3. One welded mesh layer’s volumetric ratio ($V = 0.0030$).
4. Two welded mesh layer’s volumetric ratio mesh ($V = 0.0061$).

5.4 Finite Elements Results

The analysis of finite elements performed on the created models looks at the yielding of the reinforcement steel, cracking, and beam failure strength. Using the Newton–Raphson technique of analysis, the nonlinear response is calculated. Up until un-convergence, or failure, the loading was gradually raised. Table 7 lists the results of the finite element analysis predictions, including the final loads and deflection.

For group A, the reactive powder concrete specimen (A2) was slightly better than the concrete specimen (A1) in terms of strength, where the ultimate load of the specimen (A2) was higher by 9.5% compared to specimen (A1), while no noticeable difference was observed between the two samples in terms of deflection values, and this is relatively consistent with experimental results.

The numerical results confirmed the same previously observed effects of the study factors from the experimental results, as they showed that the use of EMM was better than WWM, as the maximum load increased by rates ranging from 6.2 to 7.1%, and multiplying the number of layers in the mesh led to an increase in the maximum load by rates ranging from 3.4 to 10.9%, and the use of

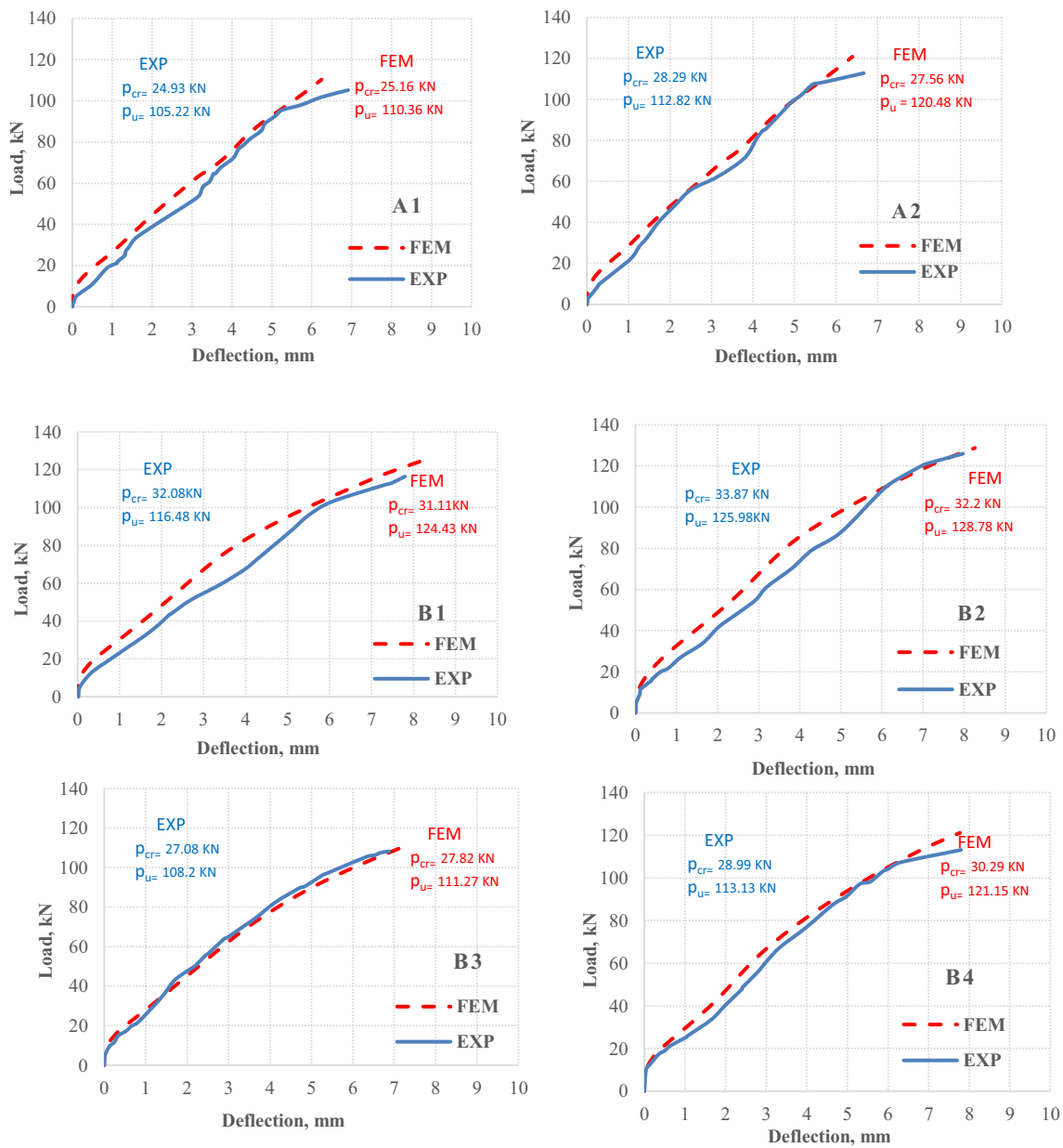


Fig. 20 Comparison between experimental and numerical load–deflection curves for all beams

AAC instead of EFC led to a slight increase in the maximum load by rates ranging from 1.6 to 3.2%. As for the ductility improved slightly with the use of EMM and increased the number of mesh layers. However, no clear effect was observed with the type of void material on the ductility coefficient. These results are consistent with Erfan and Elsayed’s research (Erfan & El-Sayed, 2019a).

5.5 Cracking Patterns and Mode of Failure

Fig. 17 depicts the modes of failure and cracking forms for all specimens’ finite element models. All specimens collapsed as a shear failure.

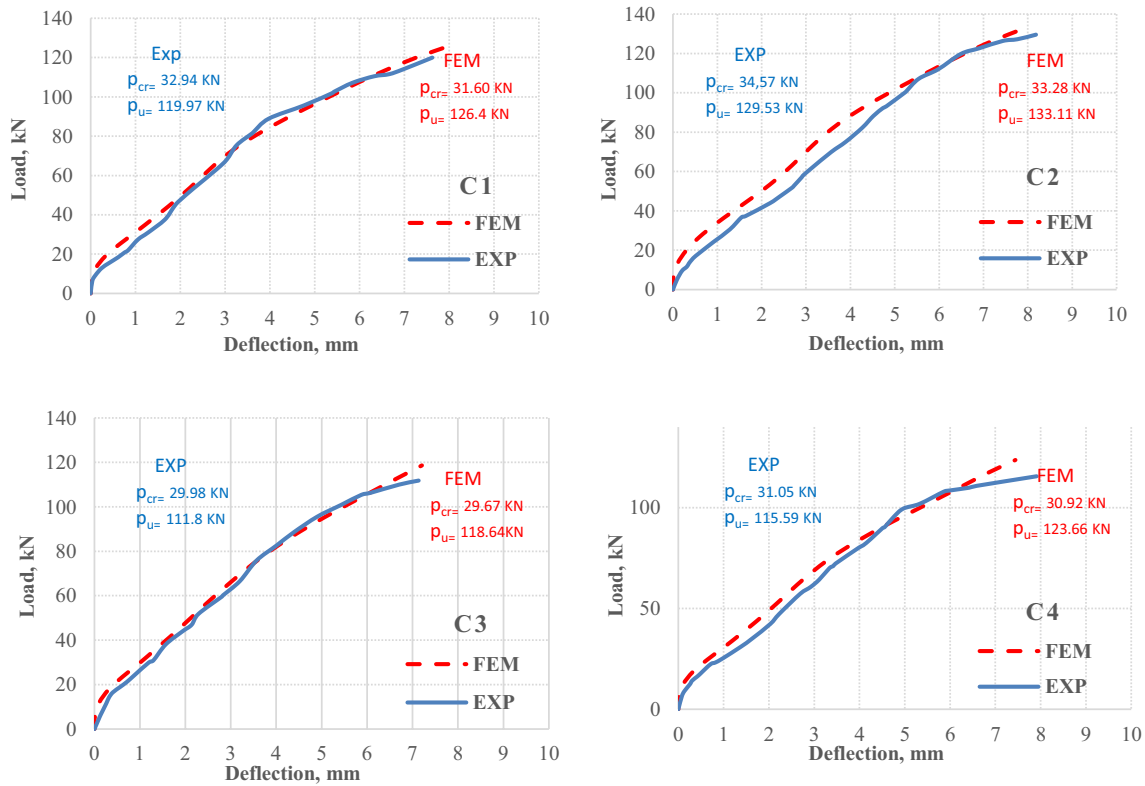


Fig. 20 continued

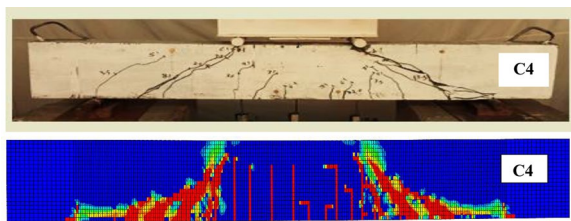


Fig. 21 Sample crack pattern for EXP & NLFE

6 Contrast of Experimental and Nlfea Results

To confirm that NLFE models are appropriate for depicting the behavior and response of the ferrocement beams, experimental and nonlinear finite element data are compared. In terms of ultimate deflection, crack pattern, and ultimate load, the ten analytical methods were contrasted with the experimental findings.

6.1 Ultimate Load

Table 8 and Fig. 18 show commendable communication between the experimental ultimate load and the equivalent value from the NLFE study. The ratio of the experimental ultimate loads to the NLFE ultimate loads falls between 1.02 and 1.07, with 1.04 being the norm. This

demonstrates the NLFE's capability to forecast the load-bearing capacity of reinforced cement beams with light core materials.

6.2 Ultimate Deflection

Table 8 and Fig. 19 demonstrate a commendable agreement between the analytical ultimate deflection produced from the NLFE program and the experimental ultimate deflection. The ratio of the experimental ultimate deflections to the NLFE ultimate deflections falls between 0.9 and 0.96, with 0.93 being the average. This confirms that the NLFEA can predict the ultimate deflection of ferrocement beams with lightweight core material.

6.3 Comparison of Load–Deflection Curves

Fig. 20 contrasts the experimental and calculated load–deflection curves for every specimen.

6.4 Crack Patterns

Fig. 21 shows a comparison example between the cracking patterns of experimental and numerical specimens. The figure reveals a similarity between both cracking patterns, where cracks start as microcracks in flexural and increase in length and width until failure as a shear failure.

7 Conclusions

The main conclusions can be drawn as follows:

1. Particularly in box beams, expanded and welded wire mesh has shown advantages over traditional reinforcing steel reinforcement, including high strength, simple handling, shape-ability, and low weight.
2. The ferrocement specimens with AAC core material and reinforced by two layers of EMM have the highest ultimate load and also the highest maximum deflection, which is higher than the convention-reinforced concrete specimen (control specimen A1) by 12.9% and 22.8%, respectively.
3. Using expanded or welded wire mesh instead of steel stirrups exhibits a high ultimate load at a rate ranging from 3.2 to 13% over the control specimen.
4. The use of EMM was slightly better than WWM, as the maximum load increased by rates ranging from 2.9 to 3.8%.
5. Increasing the expanded and welded wire mesh's layer count from one layer to two layers improved the ultimate load by 3.4 to 8.1%.
6. The proposed finite element models revealed an acceptable agreement with the experimental, where the ratio between the NLFE ultimate loads to the experimental ultimate varies between 1.02 and 1.07, with an average ratio of 1.04.

Acknowledgements

Not applicable.

Author contributions

M.H.M: design the experimental program methodology, perform the experimental program and final draft, M.A: perform the experimental program, numerical modeling, and original draft, G. I. K: design the experimental program methodology, review and editing, K. M. E: design the experimental program methodology, review and editing, M.M: numerical modeling, review, and editing. All authors read and approved the final manuscript.

Funding

Open access funding provided by The Science, Technology & Innovation Funding Authority (STDF) in cooperation with The Egyptian Knowledge Bank (EKB). Not applicable.

Availability of data and materials

All data generated or analyzed during this study are included in this published article.

Declarations

Ethics approval and consent to participate

Not applicable.

Consent for publication

Not applicable.

Competing interests

There is no competing interest associated with the submission of this manuscript.

Received: 12 December 2023 Accepted: 27 March 2024

Published online: 31 July 2024

References

- Abang, A. A. A. (1995). Application of ferrocement as a low-cost construction material in Malaysia. *Journal of Ferrocement*, 25(2), 123.
- Abaqus. (2013). Abaqus user's guide, Abaqus documentation user's guide. Dassault Systems, Simulia Corp.
- Abdallah, A. H., Erfan, A. M., El-Sayed, T. A., & Abd El-Naby, R. M. (2019). Experimental and analytical analysis of lightweight ferrocement composite slabs. *Engineering Research Journal*, 1(41), 73–85.
- Abdullah, Q. N., & Abdulla, A. I. (2022). Flexural behavior of hollow self-compacted mortar ferrocement beam reinforced by GFRP bars. *Case Studies in Construction Materials*, 17, e01556.
- Abdullah, Q. N., & Abdulla, A. I. (2023). Flexural behavior of a box ferrocement beams consisting of self-compacted mortar reinforced by fiber glass mesh and GFRP bars after exposure to high temperatures. *Journal of Building Engineering*, 74, 106917. <https://doi.org/10.1016/j.jobe.2023.106917>
- ACI 549.1R-93, & ACI 549-1R-88. (1999). A. C. I. guide for the design construction, and repair of ferrocement, ACI Committee 549.1R-93; ACI 549-1R-88 and 1R-93.
- Acma, L., & Mariano, C. (2014). Development and application of ferrocement I-beams (Doctor of Engineering Dissertation, Philippines: MSUIT, Iligan City).
- Adam, M. A., Erfan, A. M., Habib, F. A., & El-Sayed, T. A. (2021). Structural behavior of high-strength concrete slabs reinforced with GFRP bars. *Polymers*, 13(17), 2997.
- Al-Numan, B. S., Farhan, J. A., & Ali, O. K. (2016). Flexural strength and ductility of CFRP strengthened reinforced concrete beams. *Engineering and Technology Journal*, 34, 1294–1307.
- Alobaidy, Q. N. A., Abdulla, A. I., & Al-Mashaykhi, M. (2022). Shear behavior of hollow ferrocement beam reinforced by steel and fiberglass meshes: Shear behavior. *Tikrit Journal of Engineering Sciences*, 29(4), 27–39.
- Al-Shathir, B. S., Abdulhameed, H. A., & Mahdi, M. M. (2022). Effect of wire-mesh type on strengthening reinforced concrete beams. *Engineering and Technology Journal*, 40(05), 759–768.
- Al-Sulaimani, G. J., Basunbul, I. A., & Mousselly, E. A. (1991). Shear behavior of ferrocement box beams. *Cement and Concrete Composites*, 13(1), 29–36.
- ASTM C 494/C494M. (2005). Standard specification for chemical admixtures for concrete.
- ASTM C/150-07. (2007). Standard specification for Portland cement.
- ASTM C778. (2021). Graded sand ASTM cement testing standard specifications for standard sand'.
- E.C.P. 203. (2020). Egyptian code of practice: Design and construction for reinforced concrete structures, Egypt Cairo.
- Egyptian Standards Specification, E.S.S, 4756-11. (2012). Physical and mechanical properties examination of cement, part 1, Cairo.
- El-Sayed, T. A. (2021). Axial compression behavior of ferrocement geopolymer hsc columns. *Polymers*, 13(21), 3789.
- El-Sayed, T. A., & Algash, Y. A. (2021). Flexural behavior of ultra-high performance geopolymer RC beams reinforced with GFRP bars. *Case Studies in Construction Materials*, 15, e00604.
- El-Sayed, T. A., Deifalla, A. F., Shaheen, Y. B., Ahmed, H. H., & Youssef, A. K. (2023c). Experimental and numerical studies on flexural behavior of GGBS-based geopolymer ferrocement beams. *Civil Engineering Journal*, 9(3), 629–653.
- El-Sayed, T. A., & Erfan, A. M. (2018). Improving shear strength of beams using ferrocement composite. *Construction and Building Materials*, 172, 608–617.
- El-Sayed, T. A., Erfan, A. M., Abdelnaby, R. M., & Soliman, M. K. (2022). Flexural behavior of HSC beams reinforced by hybrid GFRP bars with steel wires. *Case Studies in Construction Materials*, 16, e01054.
- El-Sayed, T. A., Shaheen, Y. B., AbouBakr, M. M., & Abdelnaby, R. M. (2023a). Behavior of ferrocement water pipes as an alternative solution for steel water pipes. *Case Studies in Construction Materials*, 18, e01806.
- El-Sayed, T. A., Shaheen, Y. B., Mohamed, F. H., & Abdelnaby, R. M. (2023b). Performance of ferrocement composites circular tanks as a new approach for RC tanks. *Case Studies in Construction Materials*, 19, e02228.

- Erfan, A. M., Abd Elnaby, R. M., Badr, A. A., & El-Sayed, T. A. (2021a). Flexural behavior of HSC one-way slabs reinforced with basalt FRP bars. *Case Studies in Construction Materials*, 14, e00513.
- Erfan, A. M., Abd Elnaby, R. M., Elhawary, A., & El-Sayed, T. A. (2021b). Improving the compressive behavior of RC walls reinforced with ferrocement composites under centric and eccentric loading. *Case Studies in Construction Materials*, 14, e00541.
- Erfan, A. M., Ahmed, H. H., Mina, B. A., & El-Sayed, T. A. (2019a). Structural performance of eccentric ferrocement reinforced concrete columns. *Nanoscience and Nanotechnology Letters*, 11(9), 1213–1225.
- Erfan, A. M., Algashb, Y. A., & El-Sayed, T. A. (2019b). Experimental and analytical behavior of HSC columns reinforced with basalt FRP BARS. *International Journal of Scientific and Engineering Research*, 10(9), 240–260.
- Erfan, A. M., & El-Sayed, T. A. (2019a). Structural shear behavior of composite box beams using advanced innovated materials. *Journal of Engineering Research and Reports*, 5, 1–14.
- Erfan, A. M., & El-Sayed, T. A. (2019b). Shear strength of ferrocement composite boxsection concrete beams. *International Journal of Scientific and Engineering Research*, 10, 260–279.
- Fahmy, E. H., Shaheen, Y. B. I., Abdelnaby, A. M., & Abou Zeid, M. N. A. (2014). Applying the ferrocement concept in construction of concrete beams incorporating reinforced mortar permanent forms. *International Journal of Concrete Structures and Materials*, 8(1), 83–97.
- Fouad, E. A., John, N. M., & Charles, K. K. (2020). Openings effect on the performance of reinforced concrete beams loaded in bending and shear. *Engineering, Technology, and Applied Science Research*, 10(2), 5352–5360.
- Gaidhankar, D. G., Kulkarni, M. S., & Jaiswal, A. R. (2017). Ferrocement composite beams under flexure. *International Research Journal of Engineering and Technology*, 04(10), 117–124.
- Kaish, A. B. M. A., Jamil, M., Raman, S. N., Zain, M. F. M., & Nahar, L. (2018). Ferrocement composites for strengthening of concrete columns: A review. *Journal of Construction and Building Materials*, 160, 326–340.
- Naaman, A. E. (2015). Ferrocement: Progress review and critical need for the future. In *11th international symposium on ferrocement and textile reinforced concrete* (pp. 9–14).
- Naser, F. H., Al Mamoori, A. H., & Dhahir, M. K. (2021). Effect of using different types of reinforcement on the flexural behavior of ferrocement hollow core slabs embedding PVC pipes. *Ain Shams Engineering Journal*, 12(1), 303–315.
- Nasr, N. E. (2019). Strengthening of RC beams using different techniques. *IOSR Journal of Mechanical and Civil Engineering*, 16, 72–82. <https://doi.org/10.9790/1684-1601027282>
- Nassif, H., & Najm, H. (2004). Experimental and analytical investigation of ferrocement-concrete composite beams. *Cement and Concrete Composites*, 26, 787–796.
- Nassif, M. K., Erfan, A. M., Fadel, O. T., & El-Sayed, T. A. (2021). Flexural behavior of high strength concrete deep beams reinforced with GFRP bars. *Case Studies in Construction Materials*, 15, e00613.
- Rao, T. C., Rao, T. D. G., & Rao, N. V. R. (2006). An appraisal of the shear resistance of ferrocement elements. *Asian Journal of Civil Engineering (Building and Housing)*, 7(6), 591–602.
- Shaaban, I. G., Shaheen, Y. B., Elsayed, E. L., Kamal, O. A., & Adesina, P. A. (2018a). Flexural characteristics of lightweight ferrocement beams with various types of core materials and mesh reinforcement. *Construction Building Materials*, 171, 802–816.
- Shaaban, I. G., Shaheen, Y. B., Elsayed, E. L., Kamal, O. A., & Adesina, P. A. (2018b). Flexural behaviour and theoretical prediction of lightweight ferrocement composite beams. *Case Studies in Construction Materials*, 9, e00204. <https://doi.org/10.1016/j.cscm.2018.e00204>
- Shaheen, Y. B. I., El-Sabbawy, M., & El-Bordeny, D. A. H. (2022). Structural characteristics of lightweight ferrocement beams with different core material. *Journal of Engineering Research and Reports*, 23(6), 30–52.
- Suresh, V. (2004). Application of ferrocement for cost-effective building construction. *Journal of Ferrocement*, 34(4), 445–455.
- Usman, F., & Shaharudin, M. S. (2018). Effect of polypropylene fibres on torsional strength of ferrocement. *Indian Journal of Science and Technology*. <https://doi.org/10.17485/ijst/2018/v11i8/114093>
- Yardim, Y. (2019). Review of research on the application of ferrocement in composite precast slabs. *Periodica Polytechnica Civil Engineering*, 62(4), 1030–1038.

Publisher's Note

Springer Nature remains neutral with regard to jurisdictional claims in published maps and institutional affiliations.

Mohamed H. Makhlouf is an Associate Professor of the Civil Engineering Department at Benha Faculty of Engineering, Benha University, Egypt.

M. Alaa is a Ph.D. Student, Civil Engineering Department, Benha Faculty of Engineering, Benha University, Egypt.

I. K. Gamal is a Professor Civil Engineering Department, Benha Faculty of Engineering, Benha University, Egypt.

K. M. Elsayed is a professor in the civil engineering department of Benha Faculty of Engineering at Benha University, Egypt.

M. H. Mansour is an Assistant Professor in the Civil Engineering Department at Benha Faculty of Engineering, Benha University, Egypt.